THE JOURNAL OF PHYSICAL CHEMISTRY C

Article

Cite This: J. Phys. Chem. C 2019, 123, 11677−11685

pubs.acs.org/JPCC

Electrochemistry of the Basal Plane versus Edge Plane of Graphite Revisited

Published as part of The Journal of Physical Chemistry virtual special issue "Young Scientists".

Matěj Velický,*[,†,‡,§] Peter S. Toth,[†,∥] Colin R. Woods,[‡] Kostya S. Novoselov,[‡] and Robert A. W. Dryfe*[,†]

[†]School of Chemistry and [‡]School of Physics and Astronomy, University of Manchester, Oxford Road, Manchester M13 9PL, United Kingdom

[§]Department of Chemistry and Chemical Biology, Cornell University, Ithaca, New York 14853, United States

[∥]MTA Premium Post Doctorate Research Program, Department of Physical Chemistry and Materials Science, University of Szeged, Rerrich Square 1, Szeged H-6720, Hungary

Supporting Information

ABSTRACT: The electrochemical activity of the basal plane and edge plane of graphite has long been a subject of an extensive debate. While significant advances have been made, several gaps still exist in our understanding of this issue, namely, the relative differences in the electrochemical activity of the perfect basal plane and perfect edge plane and the dependence of measurable electrochemical quantities on the edge/defect density of the basal plane. In this work, we employ a microdroplet electrochemical cell technique and atomic force microscopy to measure localized electrochemical properties of the graphitic surface with known edge coverage. The electron transfer rate, capacitance, and density of electronic states of the perfect basal plane and perfect edge plane are estimated, and a qualitative model is proposed for the dependence of the electrochemical quantities on the defect density of the basal plane.

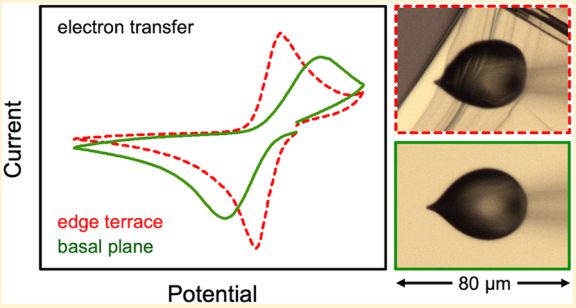

INTRODUCTION

Electrochemistry of graphite has been studied by numerous researchers since the 1960s for its utility as a low-density, chemically stable, and affordable material.[1,2] Its most common forms include natural graphite (NG) and highly oriented pyrolytic graphite (HOPG), both of which consist of sp^2 hybridized carbon atoms, covalently bound in a planar hexagonal lattice. These two-dimensional graphene planes stack on top of each other due to the weak attractive van der Waals forces to form the three-dimensional lattice of graphite. The surface parallel to the graphene planes is called the basal plane, while the perpendicular surface is called the edge plane (Figure 1). The basal plane surface is characterized by its atomic flatness and low defect density, while the edge plane surface contains sp^3 sites, defects, dangling bonds, and functional groups, owing to the abrupt lattice termination.

The debate concerning the electrochemical activity of the basal plane versus that of the edge plane of graphite has been sustained for many decades until the present day. The first level of analysis revealed that while the edge plane is the electrochemically active part of graphitic surfaces, the basal plane either has a vanishingly low electrochemical activity or is completely inactive, as inferred from capacitance, electron transfer (ET), and adsorption measurements.[3−9] Specifically, the upper limit of the standard heterogeneous ET rate (k^0) of the ferro/ferricyanide redox mediator was estimated to be 10^{-9}−10^{-7} cm s^{-1}.[7,9] Contrasting evidence was put forth later, suggesting that the basal plane of HOPG might have an intrinsic activity, with orders of magnitude higher k^0 values than previously reported.[10,11] Most recent advances in localized electrochemical measurements, electrochemical imaging, and surface preparation shed new light on this debate, confirming unequivocally that the edges and defects are more active than the basal plane[12−14] but demonstrating that the basal plane has a non-negligible electrochemical activity.[15−20]

Graphite is a semimetal with a small overlap (~60 meV) between the valence and conduction bands and a roughly parabolic dependence of the density of electronic states (DOS) on energy on either side of the Fermi level (E_F).[21,22] The DOS is generally low enough for graphite to exhibit a space charge-dominated capacitance response when in contact with electrolyte solutions, in contrast to metals.[5,23] It therefore follows that the dangling bonds, impurities, and surface groups found at the edges/defects are likely to increase the surface DOS and therefore locally enhance the capacitance or ET, especially near the DOS minimum at the E_F. Indeed, scanning tunneling

Received: January 31, 2019
Revised: April 11, 2019
Published: April 17, 2019

DOI: 10.1021/acs.jpcc.9b01010
J. Phys. Chem. C 2019, 123, 11677−11685

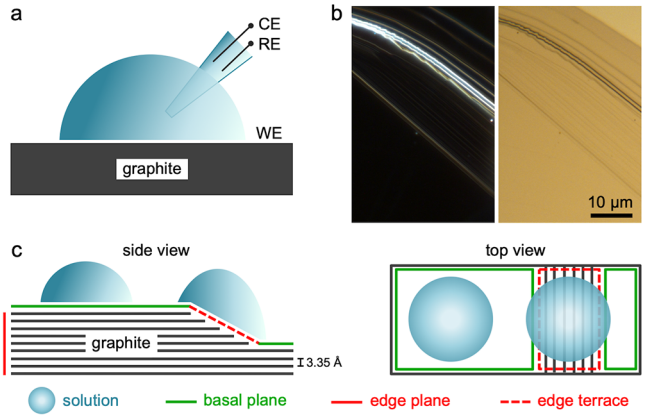

Figure 1. Schematic of the electrochemical setup and the two surface types of graphite. (a) Schematic of the microdroplet electrochemical cell on graphite (side-view). (b) High-resolution dark-field (left) and bright-field (right) optical images of the basal plane (bottom-left half) and edge terraces (top-right half). (c) Side-view and top-view schematics of the microdroplets on the basal plane (green) and edge terrace (red) surfaces.

microscopy (STM) measurements and first-principles calculations revealed localized states within 1−2 nm from the edges and a sharp peak in the DOS near the E_F for graphene/graphite.[24−28]

A common observation is that the electrochemical response varies vastly, even for graphitic surfaces prepared using the same method.[29−31] It has been shown that only a high quality sp^2 basal plane surface can provide quantitative insights into the differing ET activity of the edge/basal plane, as even seemingly low coverage of the surface by the significantly more active edges will dominate the measured response entirely.[9,32] For this reason, many researchers utilized HOPG, whose highest quality variants have a typical spacing of 1−10 μm between single crystal domains.[9,33] Although not used extensively until recently, NG has long been identified as a suitable material for fundamental electrochemical studies due to its large single crystal domains and low doping levels.[2] Recent advances in graphene/graphite electrode preparation from NG, combined with a microdroplet measurement, have enabled the acquisition of localized electrochemical responses from single crystal domains with lateral dimensions of 50−400 μm.[34,35]

It is particularly advantageous to study the ET for outer-sphere redox systems, which are sensitive to the DOS of the electrode and the electronic coupling between the electrode and redox mediator, but not to the specific surface groups as is the case for the inner-sphere systems.[31,36,37] An outer-sphere redox mediator therefore serves as a direct probe of the surface DOS of graphite, without specific sensitivity to its surface chemistry. This has however been opposed by Zhang et al., who asserted that since the DOS of the semimetallic graphite is orders of magnitude higher than that of the redox species, any variation in the DOS is unimportant.[38] A useful analysis was offered by McCreery and McDermott, who concluded that the three main factors influencing the ET rate are the redox mechanism, surface DOS, and presence of edge plane.[23] We add that another important factor is the contamination of graphitic surfaces upon exposure to ambient conditions which rapidly decreases the ET rate by several orders of magnitude.[11,35,39−42]

This work aims to provide further experimental insights into the basal versus edge plane phenomenon and to synthesize it with the literature to date. It transpires from the above analysis that two main ingredients needed for a detailed experimental examination of the electrochemical differences between the basal plane and edge plane of graphite are a high-quality surface with well-defined morphology and a localized electrochemical measurement. To that end, we study the ET and capacitance on high-quality, single crystal graphite using a localized microdroplet electrochemical cell measurement and estimate the edge coverage of the measured area from atomic force microscopy (AFM) in order to isolate the relative contributions of the perfect basal plane and perfect edge plane of graphite.

METHODS

Materials and Chemicals. Natural graphite crystals ("graphenium" grade) were purchased from NGS Naturgraphit GmbH. All metals were obtained from Advent Research Materials UK. Acetone (≥99%), isopropanol (≥99%), ammonium hexachloroiridate(IV) (≥99.9%), hexaammineruthenium(III) chloride (≥98%), potassium ferricyanide(III) (≥99%), and lithium chloride (≥99%) were purchased from Sigma-Aldrich UK and used as received. All aqueous solutions were prepared using 18.2 MΩ cm resistivity water, deionized by Milli-Q Direct 8 (Merck Millipore).

Graphite Preparation and Characterization. Graphite flakes with a typical thickness of ∼1 μm were mechanically exfoliated from bulk NG onto SiO_2/Si wafers (IDB Technologies Ltd. UK) as described previously.[35,40] The wafers were previously cleaned by sequential sonication in acetone and isopropanol (both 10 min) and by O_2/Ar plasma ashing. A Nikon Eclipse LV100ND optical microscope with a DS-Fi2 U3 CCD camera (both Nikon Metrology, UK Ltd.) was employed to acquire bright- and dark-field optical images. Surface topography of the graphite flakes was characterized by AFM in tapping mode using a Bruker Dimension 3100 V model (Bruker UK Ltd.). Raman spectroscopy, carried out using an inVia spectrometer with a 532 nm laser excitation (Renishaw plc UK) focused via a 100× Leica objective to ∼0.8 μm^2 spot size, was used to assess the surface defect density. The X-ray photoelectron spectroscopy (XPS) measurement were obtained using an AXIS Nova surface analysis spectrometer with a monochromated Al Kα X-ray source and spatial resolution of $<(3 \times 3)$ μm^2 (Kratos Analytical Ltd. UK).

Electrochemical Measurements. The electrochemical characterization of graphite was carried out using the recently introduced microdroplet electrochemical cell.[35,40] Briefly, a microdroplet of a 6 M LiCl aqueous solution (22−37 μm in diameter), either pure or containing the redox mediator of interest, was dispensed via a glass capillary using a pneumatic pressure controller and handled using an electronic micromanipulator. The capillary contained both the Ag/AgCl reference electrode (RE) and Pt counter electrode (CE), while the contact area between the microdroplet and the graphitic surface acted as the working electrode (WE), as schematically shown in Figure 1a. This three-electrode configuration was controlled by a PGSTAT302N potentiostat (Metrohm Autolab). Cyclic voltammetry in pure 6 M LiCl supporting electrolyte at scan rates in the range of 0.1−3.0 V s^{-1} was employed to measure the average interfacial capacitance (C_{int}), calculated by the current integration over the applied potential range (−0.2 to 0.7 V), using eq 3 in ref 43. Cyclic voltammograms of the redox mediators recorded at scan rates in the range of 0.1−3.0 V s^{-1} (Figure S1) were used to evaluate k^0, which was calculated using eq 26 in ref 44 for the peak-to-peak separation (ΔE_p) larger than 220 mV or eq 2 in ref 45 for ΔE_p <

DOI: 10.1021/acs.jpcc.9b01010
J. Phys. Chem. C 2019, 123, 11677−11685

220 mV, and averaged over the applicable scan rate range. The mean diffusion coefficients of $(2.7 \pm 0.1) \times 10^{-6}$ cm^2 s^{-1} for $[IrCl_6]^{2-/3-}$ and $(2.4 \pm 0.1) \times 10^{-6}$ cm^2 s^{-1} for $[Ru(NH_3)_6]^{3+/2+}$, used for the k^0 calculation, are averages of the diffusion coefficients of their reduced and oxidized forms, measured by cyclic voltammetry and chronoamperometry at polished Pt disk macroelectrode using the Randles−Ševčík and Cottrell equations, respectively.[37] All measurements were carried out within the temperature range of 295−301 K.

RESULTS AND DISCUSSION

Selection and Characterization of the Graphitic Surfaces. In order to directly compare the electrochemical response of the basal plane and edge plane of graphite, we mechanically exfoliated a single crystal of graphite with well-defined basal plane and edge terrace regions as exemplified by the optical images in Figure 1b. A microdroplet of solution is then placed on either the basal plane or edge terrace surface, as shown schematically in Figure 1c, allowing for a localized electrochemical measurement at the region of interest. Such methodology has several advantages.

Carefully chosen NG crystals far exceed in quality the best HOPG, assessed by their aforementioned large single crystal domain spacing. The Raman spectrum of a high-quality basal plane HOPG is free of the defect-activated D band, which is otherwise present in disordered materials such as glassy carbon.[46] Indeed, no D band can be seen in the Raman spectra of the basal plane of our NG graphite, while the edge terraces exhibit a noticeable D band, as shown in Figure 2a. However, the

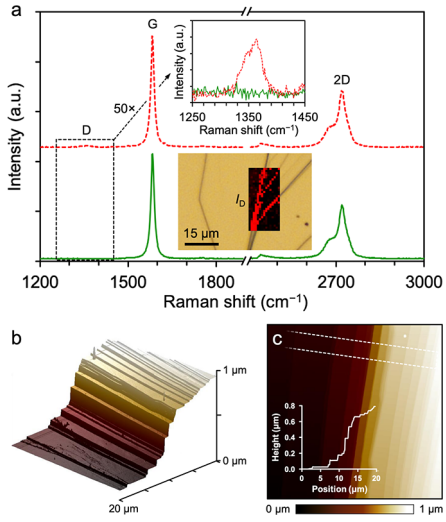

Figure 2. Raman spectroscopy and AFM characterization of graphite. (a) Raman spectra of the basal plane (green) and edge terraces (red). The top inset shows a magnified region with the defect-activated D band. The bottom inset shows a map of the D band intensity (I_D), overlaid over an optical image of the region of interest. (b) 3D AFM image of the edge terrace in Figure 1b. (c) 2D AFM image of the same region. The inset graph shows the height profile of the terrace from the region highlighted by the dashed lines.

average purity of our NG determined by XPS is ∼93%, with the bulk and adsorbate impurities consisting mainly of O (<5%), N (1<%), F (<1%), and Si (<1%),[40] which is somewhat lower than for a typical HOPG (∼99%).[47] The XPS mapping showed no significant heterogeneity in the distribution of the major elements across the surface of the edge terraces and basal planes (Figure S2). While these impurities are likely to systematically alter the average electrochemical response in comparison to HOPG, they are unlikely to cause variation between individual microdroplet measurements, averaged over areas of 400−1100 μm^2.

Another important characteristic of our system is the proximity of the locations of the measurements on the basal plane and edge terrace, which ensures that the applied potential is essentially identical for both surface types, regardless of any contact or sample resistance, and the directly comparable electrochemical responses therefore differ only due to the changes in the surface DOS. The microdroplet technique employed here is an intermediate between the conventional macroscale electrochemistry and scanning electrochemical cell microscopy, with their typical supermillimeter and submicrometer resolutions, respectively.

The gradual sloping of the selected edge terraces, exemplified by the AFM images in Figure 2b,c, results in a similar geometry for the edge and basal plane measurements. The overall step of the edge terraces is kept below 1 μm, which is negligible in comparison to the microdroplet size and thus minimizes unwanted diffusional effects due to surface topography. Furthermore, we used the AFM results to calculate the average edge coverage at the terraces, which varied between 3 and 5% and was used to estimate the electrochemical quantities of the ideal homogeneous surfaces, i.e., the perfect basal plane and perfect edge plane.

Finally, we note that all the surfaces were aged in air for at least 24 h, and it was assumed that the deterioration of the capacitance and ET rate due to the accumulation of airborne organic contaminants progressed uniformly across the entire surface and reached saturation at the time of the measurement.[39,48]

Capacitance and Potential Window of the Basal Plane and Edge Plane of Graphite. Figure 3a,b shows cyclic voltammograms on the basal plane and edge terrace of graphite in a 6 M LiCl aqueous solution, which were used to determine the interfacial capacitance (C_{int}). It is evident that C_{int}, proportional to the current density, is higher for the edge terraces with only about 5% edge coverage, compared to that for the basal plane. The C_{int} averaged from several measurements across the 0.9 V window yields 1.8 μF cm^{-2} for the basal plane and 2.8 μF cm^{-2} for the edge terrace. Similar values of 1−2 μF cm^{-2} for the basal plane were previously obtained for HOPG.[7,8] The high concentration of the 6 M LiCl supporting electrolyte has several advantages. It prevents evaporation of the microdroplet, which would lead to undesirable concentration gradient and convection effects. It suppresses side reactions on the graphitic surface, thus allowing the integration of the non-faradaic capacitive current over a wide voltage range (0.9 V). Finally, it collapses the electrical double-layer contribution to C_{int} to a single component, the Helmholtz layer capacitance (C_H). We can therefore estimate the space charge capacitance (C_{SC}) of the basal plane of graphite, reflecting its surface DOS, from the following expression for capacitance in series:[5,49]

$$\frac{1}{C_{int}} = \frac{1}{C_{SC}} + \frac{1}{C_H} \quad (1)$$

where $C_H = 25$ μF cm^{-2}, determined as C_{int} of a Pt electrode in the same system (for metals $C_{SC} \gg C_H$ and therefore $C_{int} \approx C_H$).[50] For simplicity, we ignore the potential dependence of C_{SC} and use the averaged C_{int} for the calculation. Note that the E_F of unbiased graphite corresponds to ca. − 0.13 V on the potential

DOI: 10.1021/acs.jpcc.9b01010
J. Phys. Chem. C 2019, 123, 11677−11685

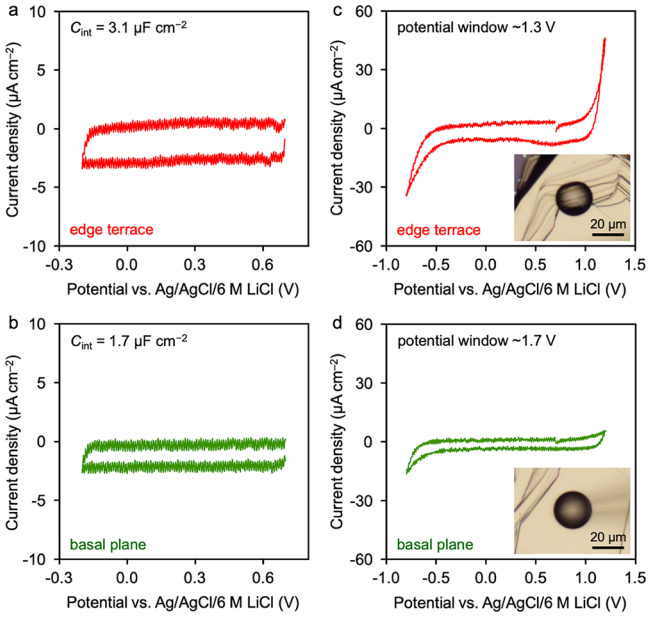

Figure 3. Capacitance and potential window of the basal plane and edge terrace of graphite. (a, b) Capacitance measurement of the edge terrace (red) and basal plane (green) of graphite measured by cyclic voltammetry in 6 M LiCl at scan rate of 0.5 V s^{-1}. The vertical areal component of the edge terrace was taken into the account when calculating the current density and C_{int}. (c, d) Potential window of the edge terrace (red) and basal plane (green) of graphite measured by cyclic voltammetry in 6 M LiCl at scan rate of 1.0 V s^{-1}, whose width was arbitrarily estimated as a potential range, for which the current density remains within ±7 μA cm^{-2}. The insets show the microdroplets on the surface, employed to obtain these measurements.

scale used here.[22,40,51] Equation 1 yields an average C_{SC} of 1.9 μF cm^{-2} for the basal plane, from which we can estimate the charge carrier concentration $n = 1 \times 10^{18}$ cm^{-3}, using the following expression:[2]

$$n = \left(\frac{C_{SC}}{e}\right)^2 \frac{k_B T}{2\varepsilon\varepsilon_0} \quad (2)$$

where k_B is the Boltzmann constant, T is the temperature, e is the elementary charge, $\varepsilon = 3.3$ is the relative static permittivity of the basal plane of graphite,[52] and ε_0 is the permittivity of vacuum. We can also estimate the average DOS of the basal plane as $\overline{\rho}_{bas} = 7 \times 10^{-4}$ states atom^{-1} eV^{-1} using the following expression:[5]

$$\overline{\rho}_{bas} = \frac{C_{SC}^2}{\varepsilon\varepsilon_0 e} \quad (3)$$

Despite being calculated from capacitance averaged for a range of potentials/energies, these values are much lower than those calculated previously using the same method for the DOS minimum at the E_F of stress-annealed pyrolytic graphite ($C_{SC} = 3$ μF cm^{-2}, $n = 11 \times 10^{18}$ cm^{-3}, and $\overline{\rho}_{bas} = 2.2 \times 10^{-3}$ states atom^{-1} eV^{-1}).[3,5,53] This suggests that the basal plane of the NG used here indeed has one of the lowest defect densities.

We proceed to estimate the capacitance of the perfect basal plane of graphite (C_{bas}), i.e., the 100% homogeneous basal surface, based on the following expression:[7]

$$C_{obs} = C_{bas}(1 - \theta_{edg}) + C_{edg}\theta_{edg} \quad (4)$$

where C_{obs} is the observed capacitance of the heterogeneous surface, C_{edg} is the capacitance of the perfect edge plane of graphite, and θ_{edg} is the fraction of the heterogeneous surface covered by edges. We now substitute C_{int} for C_{obs} and make the reasonable assumption that the DOS of the perfect edge plane is high enough so that the $C_{SC} \gg C_H$. From this follows $C_{edg} \approx C_H \approx 25$ μF cm^{-2}. Using $C_{int} = C_{obs} = 3.0$ μF cm^{-2}, obtained for a single microdroplet measurement on an edge terrace with $\theta_{edg} = 0.053$, we calculate $C_{bas} = 1.7$ μF cm^{-2}. Table 1 lists all the C_{int} and C_{SC} values. One can see that C_{int} of the perfect basal plane calculated from eqs 1 and 4 for a single measurement is nearly identical with that of the average measured capacitance of the "real" basal plane.

Table 1. Capacitance of the Basal Plane and Edge Plane of Graphite

surface type	C_{int} (μF cm^{-2})	C_{SC} (μF cm^{-2})
basal plane	1.8 ± 0.1[a]	1.9 ± 0.3[b]
edge terrace	2.8 ± 0.2[a]	
perfect basal plane	1.7 ± 0.2[c]	1.9 ± 0.2[b]
perfect edge plane	25 ± 6[d]	

[a]Averaged from several measurements. [b]Calculated using eq 1. [c]Calculated using eq 4 from a single measurement. [d]Estimated as C_H, which was measured directly on a Pt electrode.

Determination of C_{SC} and related electronic characteristics of the perfect edge plane is more problematic. According to eq 1 and the $C_{SC} \gg C_H$ condition resulting from the high DOS of the edge plane, C_{int} of the perfect edge plane is dominated by C_H, which renders the value of C_{SC} inaccessible. Some previous studies reported extremely high values of C_{int} for the edge plane, ranging from 60 to 10^5 μF cm^{-2}.[4,7,54,55] However, as the analysis above shows, the maximum value that C_{int} can assume for a purely nonfaradaic capacitance is C_H, which is typically on the order of 15−40 μF cm^{-2} for most concentrated electrolytes.[56,57] Such high C_{int} values therefore do not reflect the change in the surface DOS but rather other pseudocapacitive effects such as faradaic redox processes, ion intercalation, or surface fracture leading to an increase in the electrode area.

Figure 3c,d shows cyclic voltammograms in the 6 M LiCl supporting electrolyte on the same edge and basal surfaces extended to the full potential window where the side reactions such as oxygen reduction and graphite oxidation occur. The electrochemical potential window of the basal plane appears to be ~0.4 V larger than that of the more reactive edge terrace. This direct observation of the inherent electrochemical reactivity of the edge plane is in agreement with the evidence of preferential electrochemical oxidation at the graphitic edges from STM.[58]

Electron Transfer on the Basal Plane and Edge Plane of Graphite. Figure 4a,b shows cyclic voltammograms of the $[IrCl_6]^{3-/2-}$ and $[Ru(NH_3)_6]^{2+/3+}$ oxidation/reduction on the basal plane and edge terraces of graphite, respectively. We have chosen these redox mediators, as there is no evidence of an inner-sphere mechanism in their ET.[50,59] They are both outer-sphere in nature, characterized by their insensitivity to specific surface groups, which allows us to only probe the effects of the surface DOS on the ET rate. There is an apparent difference between the two surfaces, with a smaller ΔE_p of the reduction and oxidation waves for the edge terraces, indicating faster ET rate. The average k^0 values obtained from several independent measurements are about 30 and 800 times larger on the edge terrace than on the basal plane for $[IrCl_6]^{3-/2-}$ and $[Ru(NH_3)_6]^{2+/3+}$, respectively (Table 2). This variation of k^0 on the two different surfaces with differing DOS implies that the ET is

DOI: 10.1021/acs.jpcc.9b01010
J. Phys. Chem. C 2019, 123, 11677−11685

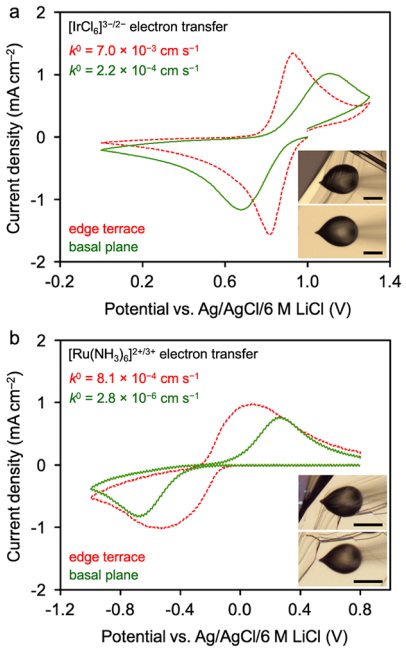

Figure 4. Electron transfer on the basal plane and edge terrace of graphite. (a, b) Oxidation/reduction of $[IrCl_6]^{3-/2-}$ and $[Ru(NH_3)_6]^{2+/3+}$, respectively, measured by cyclic voltammetry at scan rate of 1 V s^{-1} using a 3 mM mediator solution in 6 M LiCl. The responses of both the basal plane (green) and the edge terraces (red) are shown, alongside the k^0 determined from ΔE_p. The insets show the microdroplets used to perform these measurements with scale bars of 20 μm. The vertical areal component of the edge terrace was taken into the account when calculating the current density.

Table 2. Electron Transfer Rates of $[IrCl_6]^{3-/2-}$ and $[Ru(NH_3)_6]^{2+/3+}$ on Graphite

	k^0 (cm s^{-1})	
surface type	$[IrCl_6]^{3-/2-}$	$[Ru(NH_3)_6]^{2+/3+}$
basal plane	$(2.0 \pm 0.1) \times 10^{-4}$ [a]	$(1.1 \pm 0.9) \times 10^{-6}$ [a]
edge terrace	$(5.6 \pm 0.7) \times 10^{-3}$ [a]	$(8.7 \pm 2.0) \times 10^{-4}$ [a]
perfect basal plane	$(9.1 \pm 0.1) \times 10^{-5}$ [b]	$(3.7 \pm 0.6) \times 10^{-7}$ [b]
perfect edge plane	$(1.6 \pm 0.1) \times 10^{-1}$ [c]	$(1.5 \pm 0.3) \times 10^{-2}$ [c]

[a]Averaged from several measurements. [b]Extrapolated from the k^0 dependence on scan rate. [c]Calculated using eq 6 from a single measurement.

nonadiabatic, i.e., the electronic coupling between the electrode and redox mediator is weak, and the ET process is sudden. From this follows that k^0 is governed by the following relationship arising from the Marcus–Hush theory of ET:[60]

$$k^0 = \frac{2\pi^2 \rho_E^0 (H_{ER}^0)^2}{\beta h \sqrt{1 + \frac{\lambda}{\pi k_B T}}} e^{-\lambda/4k_B T} \quad (5)$$

where ρ_E^0 is the DOS of the electrode at the standard potential of the mediator (for metals, the DOS is generally assumed to be independent of potential), H_{ER}^0 is the electronic coupling matrix between the electrode and redox mediator at close contact between the two, λ is the reorganization energy of the redox mediator, β is the exponential decay coefficient of the electronic coupling, and h is the Planck constant.

It has been shown previously that (unlike the capacitance as shown above) the apparent ET rate of the basal plane cannot be fully assigned to the perfect basal plane response. This is because even for a seemingly small coverage of the low-activity basal surface by significantly more active edge/defect sites, the ET rate will be dominated, or at least significantly affected, by the active sites' contribution.[32,61] As we will see below, this is also the case for our "real" basal plane, which has the edge/defect coverage well below the 0.1–1% estimated for the basal plane HOPG previously.[32] The large k^0 of the "fast" edge plane will cause the depletion of the diffusion layer from the surrounding volume before the reaction has a chance to proceed on the "slow" basal surface. This effect can be counteracted by significantly increasing the scan rate, which reduces the diffusion layer thickness around the edges, thus gradually accessing the inherent activity of the perfect basal plane.

Some authors proposed that the basal plane might in fact be completely inactive.[8,9] However, this could only be true if the electronic coupling between the redox mediator and the basal plane were vanishingly small, since non-negligible DOS exist across the whole range of potentials except near the E_F in unbiased graphite/graphene.[22,62,63] We attempted to estimate k^0 of the perfect basal plane (k_{bas}^0), using an approach similar to that for the capacitance, based on the following expression:[7]

$$k_{obs}^0 = k_{bas}^0(1 - \theta_{edg}) + k_{edg}^0 \theta_{edg} \quad (6)$$

where k_{obs}^0 is the observed ET rate of the heterogeneous graphitic surface and k_{edg}^0 is the ET rate of the perfect edge plane of graphite. However, it became apparent that this approach is unsuitable due to the uncertainty in the determination of k_{edg}^0, as seemingly reasonable values of k_{edg}^0 can lead to nonsensical answers such as $k_{bas}^0 < 0$ or $k_{bas}^0 > k_{obs}^0$. As an example, using $[IrCl_6]^{3-/2}$ values of $k_{obs}^0 = 7.0 \times 10^{-3}$ cm s^{-1} and $\theta = 0.042$ (edge terrace in Figure 4a), and $k_{edg}^0 = 5 \times 10^{-2}$ cm s^{-1} (determined previously for laser pulse-activated HOPG),[64] yields $k_{bas}^0 = 5.1 \times 10^{-3}$ cm s^{-1}, clearly an incorrect value, since it is higher than $k_{obs}^0 = 2.2 \times 10^{-4}$ cm s^{-1} measured directly on the "real" basal plane.

To circumvent this issue, we chose a different approach based on our observation that even a very small edge/defect coverage of the basal plane is manifested by the strong dependence of the ET rate on the scan rate. We infer that this could be related to the already discussed competition between the diffusion domains of the perfect edge plane and the perfect basal plane.[7,32] At slow scan rates, the high activity of edges will cause expansion of their diffusion layer well above a significant portion of the basal plane, and the edges will dominate or substantially contribute to the measured ET rate. At fast scan rates, the diffusion layer thickness around the edges becomes small and the ET due to edges irrelevant, due to their low surface coverage. If this is so, then we can estimate k_{bas}^0 of $[IrCl_6]^{3-/2}$ by extrapolating the k_{obs}^0 obtained for the "real" basal plane in Figure 4a (green curve) to infinite scan rate (Figure S3). This yields a more realistic value of $k_{bas}^0 = 9.1 \times 10^{-5}$ cm s^{-1} for the perfect basal plane, which subsequently allows an estimation of $k_{edg}^0 = 0.2$ cm s^{-1}. The same approach yields $k_{bas}^0 = 3.7 \times 10^{-7}$ cm s^{-1} and $k_{edg}^0 = 1.5 \times 10^{-2}$ cm s^{-1} for $[Ru(NH_3)_6]^{2+/3+}$ (Figure 4b). The k_{bas}^0 values of both mediators are one of the lowest determined for the basal plane HOPG, while the k_{edg}^0 value are near to those for glassy carbon.[64] Furthermore, k_{bas}^0 and k_{edg}^0 determined this way for both mediators allowed us to estimate the edge/defect coverage of the "real" basal plane from its k_{obs}^0 and eq 6 as ca. 0.01–0.1%.

Furthermore, we use the ET data and eq 5 to estimate the DOS. Using $H_{ER}^0 = 0.1$ eV and $\beta = 1$ Å^{-1}, suggested by Feldberg and Sutin,[60] and $\lambda = 1.0$ eV for both mediators (literature values vary from 0.4 to 1.4 eV)[65–67] leads to a reasonable k^0 value of 2

DOI: 10.1021/acs.jpcc.9b01010
J. Phys. Chem. C 2019, 123, 11677–11685

cm s^{-1} for the DOS of Au (0.28 $atom^{-1}$ eV^{-1}).[36] These parameters produced the following DOS for the perfect basal plane, $\rho^{Ir}_{bas} = 1 \times 10^{-5}$ $atom^{-1}$ eV^{-1} and $\rho^{Ru}_{bas} = 6 \times 10^{-8}$ $atom^{-1}$ eV^{-1}, and for the perfect edge plane, $\rho^{Ir}_{edg} = 2 \times 10^{-2}$ $atom^{-1}$ eV^{-1} and $\rho^{Ru}_{edg} = 2 \times 10^{-3}$ $atom^{-1}$ eV^{-1}, where the ^{Ir} and ^{Ru} superscripts denote $[IrCl_6]^{3-/2}$ and $[Ru(NH_3)_6]^{2+/3+}$, respectively. Despite the uncertainty in the equation parameters and the discrepancy between the DOS determined from k^0 and C_{SC}, we can make several qualitative observations. First, the calculated DOS of the perfect edge plane appears to be 2−3 orders of magnitude lower than that of a good metal such as Au. Second, the DOS of the perfect basal plane appears to be 3−5 orders of magnitude lower than that of the edge plane. These trends are reasonable, and furthermore, the fact that $\rho^{Ru}_{bas} \ll \rho^{Ir}_{bas}$ reflects well the close proximity of the formal potential ($E^{0\prime}$) of $[Ru(NH_3)_6]^{2+/3+}$ to the DOS minimum near the E_F in unbiased graphite ($E^{0\prime}$ within 50 meV of E_F), in comparison to that of $[IrCl_6]^{3-/2}$ ($E^{0\prime}$ ca. 1 eV below E_F).

The above insights have strong implications for the shape of the cyclic voltammograms. Notably, the $[Ru(NH_3)_6]^{2+/3+}$ oxidation/reduction waves on the edge terraces (red curve in Figure 4b) are much broader than single electron transfer waves ought to be. Similar broadening was previously observed for $[Fe(CN)_6]^{4-/3-}$ and initially attributed to the dependence of the reaction transfer coefficient on potential[8] but later associated with the overlapping diffusion regions of the edge and basal planes.[9,32] The broader shape of the $[Ru(NH_3)_6]^{2+/3+}$ voltammogram on the edge terrace with ∼5% edge coverage therefore is a convolution of two simultaneous reactions on the edge and basal surfaces with significantly differing k^0. The exact shape of the voltammogram is determined by the interplay between the size of the homogeneous domains on the heterogeneous surface, relative activity of these domains, and the scan rate, as alluded to above. To further validate this explanation, we employed *in situ* exfoliation of the graphite flakes using the capillary tip, a technique which we utilized previously to study surface aging of graphite.[35] This creates a heterogeneous surface containing spatially separated homogeneous domains with differing k^0 and more balanced surface coverage. Figure 5 shows that two sets of voltammetric waves for both the fast and slow ET processes are now resolved in the cyclic voltammogram.

Furthermore, the lack of reports on similarly distorted voltammograms for $[Fe(CN)_6]^{4-/3-}$, which should be seen for a basal plane with a very low defect density as suggested by simulations, was interpreted as evidence of a completely inactive basal plane.[9,32] For a small number of cases on the basal plane NG, we did observe such distortion, including the two sets of voltammetric waves (Figure S4).

Qualitative Model of the Electrochemistry of Graphite. Here we offer a qualitative overview of the role of defects in the electrochemistry of graphite. The electronic properties of graphite are the main determining factor for the nonadiabatic, outer-sphere ET and the nonfaradaic capacitance. The DOS of the perfect basal plane is a well-defined quantity, which can be determined theoretically,[22,62] while the DOS at the edges and defects will largely depend on the edge termination and surface groups. For example, it is currently unclear if zigzag only[25,68] or both zigzag and armchair[26] terminations increase the DOS of edges, or what effects different surface groups have on the DOS. Although it has been questioned whether the low DOS of graphite is the limiting factor for the ET rate,[23,38] the conspicuous decrease of the ET rate on the basal plane in comparison to the edge plane, observed herein and elsewhere for a range of mediators, suggests that this indeed is the case and that the ET is nonadiabatic. Charge carrier mobility is another important electronic property of graphite, which has not been discussed extensively in literature to date. It has been shown that the in-plane mobility (and therefore conductivity) is over 3 orders of magnitude faster than the out-of-plane mobility.[69] The effects of mobility should be most notable for fast ET processes where large currents need to be supported by the graphite electrode.

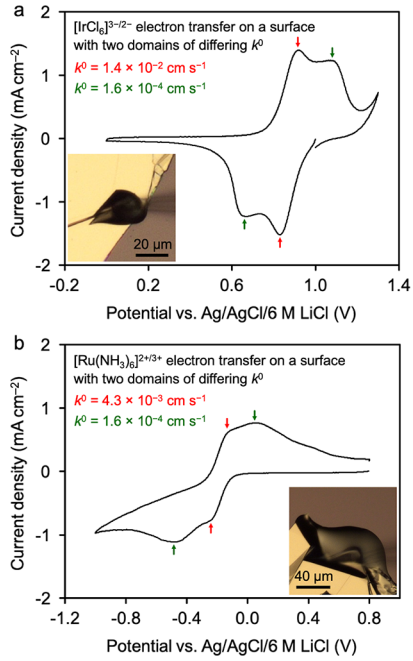

Figure 5. Electron transfer on a surface with separate domains of differing k^0. (a, b) Oxidation/reduction of $[IrCl_6]^{3-/2-}$ and $[Ru(NH_3)_6]^{2+/3+}$, respectively, measured by cyclic voltammetry at scan rate of 1 V s^{-1} using a 3 mM mediator solution in 6 M LiCl. Both responses are recorded on a heterogeneous graphitic surface with separate homogeneous domains of edge and basal plane surface, as well as the "fresh" surface exposed to the solution by the tip of the capillary. The apparent k^0 determined from the respective ΔE_p values, indicated by the red and green arrows, are also shown. The insets show the contact area between the liquid and the surface.

We propose a qualitative model of graphite electrochemistry, schematically shown in Figure 6, which relates the ET rate and capacitance with the defect density of the basal plane. The defect density can be arbitrarily expressed as the number of carbon monovacancies per surface area. Furthermore, we assume a linear dependence of the surface DOS on the defect density, based on the proportionality of both of these quantities on the surface area. Figure 6a shows a linear relationship between k^0 and the defect density, according to eq 5, for a nonadiabatic ET process. The two curves represent "fast" and "slow" redox systems, i.e., those with comparatively small and large λ, respectively, which is reflected by the differing slopes. In this simplified comparative model, we assume that $H_{ER}{}^0$ and $E^{0\prime}$ are similar for both redox systems. On the basis of our observations and review of the literature to date, we propose that k^0 of a specific redox mediator assumes a small, but nonzero value when $\theta \rightarrow 0$. This value is determined by the DOS of the perfect basal plane at the energy level corresponding to the $E^{0\prime}$ of the redox mediator. The DOS dependence on potential/energy, if shown, would add another dimension to the graph in Figure 6a, with an

DOI: 10.1021/acs.jpcc.9b01010
J. Phys. Chem. C 2019, 123, 11677−11685

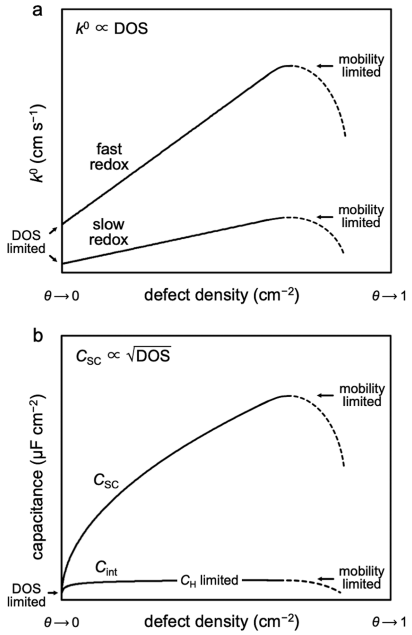

Figure 6. Schematic dependence of the electrochemical properties on the defect density of the basal plane of graphite. (a) Nonadiabatic ET rate dependence on the defect density of the basal plane, for a fast redox system with a small λ (top curve) and a slow redox system with a large λ (bottom curve). The slope of this dependence increases with the $H_{ER}{}^0$ and decreases with λ, and k^0 is limited by the DOS of the perfect basal plane when $\theta \rightarrow 0$. (b) Dependence of C_{SC} (top curve) and C_{int} (bottom curve) on the defect density of the basal plane. C_{SC} and C_{int} converge to the same, DOS-limited value for $\theta \rightarrow 0$.

approximately parabolic increase of the DOS; therefore k^0, on either side of the E_F in unbiased graphite, as discussed above. The results for $[Ru(NH_3)_6]^{2+/3+}$ suggest that the DOS, and therefore k^0, could potentially vanish to zero near the E_F in graphite/graphene. In the high defect density limit, the breakdown in the long-range crystallinity of the graphitic lattice leads to a decrease in carrier mobility, and in turn, to a decline in the ET rate. This model of k^0 dependence on defect density is supported by a direct correlation between the scanning electrochemical microscopy and Raman spectroscopy of Ar^+ irradiated graphene surface, which was achieved as a means to quantification of the ET dependence on the defect density.[14] These results revealed an approximately exponential dependence of k^0 on the logarithm of the defect density, with a sharp decline beyond $\sim 8 \times 10^{12}$ cm^{-2}, in agreement with our proposed qualitative model.

The dependence of capacitance on the defect density is schematically shown in Figure 6b. C_{SC} is proportional to the square root of DOS (and therefore to the defect density), according to eq 3. C_{int} obeys eq 1, which leads to a normalized square root dependence asymptotically approaching C_H for large DOS. Both C_{SC} and C_{int} converge to the same value for $\theta \rightarrow 0$, which is determined by the DOS of the perfect basal plane of graphite. The capacitance should also be limited by the decreasing carrier mobility in the limit of a high defect density, similar to the ET.

CONCLUSIONS

In summary, we studied the electron transfer and capacitance on natural graphite with the aim of deconvoluting the relative contributions of the perfect basal plane and perfect edge plane to these electrochemical quantities. This was achieved by a localized measurement using a microdroplet electrochemical cell deposited at locations on the graphitic surface, whose exact edge coverage was determined by AFM. We found that the perfect basal plane had a small but nonzero ET rate, while the perfect edge plane had an ET rate close to that of glassy carbon. The difference between the ET rate of the perfect basal and perfect edge plane was about 3 orders of magnitude for $[IrCl_6]^{3-/2-}$ and about 5 orders of magnitude for $[Ru(NH_3)_6]^{2+/3+}$, respectively. The interfacial capacitance in 6 M LiCl supporting electrolyte was found to increase by about an order of magnitude from the space charge capacitance limit for the perfect basal plane to the electrical double-layer limit for the perfect edge plane. The estimates from the ET and capacitance data suggested a small, but nonzero value for the DOS of the basal plane, possibly vanishing to zero near the E_F in unbiased graphite. On the basis of our results and the retrospective analysis of the relevant literature, we proposed a qualitative model for the dependence of the ET rate and capacitance on the defect density of the basal plane of graphite. Our findings offer new insights into the long-debated electrochemistry of the basal versus edge plane of graphite and serve as a guide for better utilization of graphite in fundamental research and applications.

ASSOCIATED CONTENT

Supporting Information

The Supporting Information is available free of charge on the ACS Publications website at DOI: 10.1021/acs.jpcc.9b01010.

Range of $[IrCl_6]^{3-/2-}$ cyclic voltammograms obtained at different scan rates; XPS mapping of the graphitic surface; estimation of k^0 of the perfect basal plane from its dependence on scan rate; cyclic voltammetry of $[Fe(CN)_6]^{4-/3-}$ on the basal plane (PDF)

AUTHOR INFORMATION

Corresponding Authors

*E-mail: matej.velicky@manchester.ac.uk (M.V.).
*E-mail: robert.dryfe@manchester.ac.uk (R.A.W.D.).

ORCID

Matěj Velický: 0000-0003-4230-3811
Robert A. W. Dryfe: 0000-0002-9335-4451

Notes

The authors declare no competing financial interest.

Biography

Photo by Julia Velický.

DOI: 10.1021/acs.jpcc.9b01010
J. Phys. Chem. C 2019, 123, 11677−11685

Matěj Velický is a Marie Skłodowska-Curie Global Fellow in the Department of Chemistry and Chemical Biology at Cornell University. He received a Master of Engineering degree in Nuclear Chemistry (2007) from the Czech Technical University in Prague and a Ph.D. degree in Chemistry (2011) from the University of Manchester. He was a postdoctoral research assistant at the University of Manchester and a research fellow at Queen's University Belfast before assuming his current position (2017), held jointly at Cornell University and the University of Manchester. His recent research interests span the electrochemistry of two-dimensional materials, tunable electrochemistry, and in situ characterization of electrified solid/liquid interfaces.

■ ACKNOWLEDGMENTS

This project has received funding from the UK EPSRC (grants No. EP/K007033/1 and EP/K016954/1) and the European Union's Horizon 2020 research and innovation programme under the Marie Skłodowska-Curie grant agreement No. 746685. We also thank the NEXUS service at Newcastle University for the XPS measurements.

■ REFERENCES

(1) Bauer, H. H.; Spritzer, M. S.; Elving, P. J. Double-Layer Capacity at a Pyrolytic Graphite Disk Electrode. *J. Electroanal. Chem. Interfacial Electrochem.* **1968**, *17*, 299−307.
(2) Randin, J. P.; Yeager, E. Differential Capacitance Study of Stress-Annealed Pyrolytic Graphite Electrodes. *J. Electrochem. Soc.* **1971**, *118*, 711−714.
(3) Randin, J. P.; Yeager, E. Differential Capacitance Study on the Basal Plane of Stress-Annealed Pyrolytic Graphite. *J. Electroanal. Chem. Interfacial Electrochem.* **1972**, *36*, 257−276.
(4) Randin, J. P.; Yeager, E. Differential Capacitance Study on the Edge Orientation of Pyrolytic Graphite and Glassy Carbon Electrodes. *J. Electroanal. Chem. Interfacial Electrochem.* **1975**, *58*, 313−322.
(5) Gerischer, H.; McIntyre, R.; Scherson, D.; Storck, W. Density of the Electronic States of Graphite: Derivation from Differential Capacitance Measurements. *J. Phys. Chem.* **1987**, *91*, 1930−1935.
(6) Bowling, R.; Packard, R. T.; McCreery, R. L. Mechanism of Electrochemical Activation of Carbon Electrodes: Role of Graphite Lattice Defects. *Langmuir* **1989**, *5*, 683−688.
(7) Rice, R. J.; McCreery, R. L. Quantitative Relationship between Electron Transfer Rate and Surface Microstructure of Laser-Modified Graphite Electrodes. *Anal. Chem.* **1989**, *61*, 1637−1641.
(8) McDermott, M. T.; Kneten, K.; McCreery, R. L. Anthraquinonedisulfonate Adsorption, Electron-Transfer Kinetics, and Capacitance on Ordered Graphite Electrodes: The Important Role of Surface Defects. *J. Phys. Chem.* **1992**, *96*, 3124−3130.
(9) Banks, C. E.; Davies, T. J.; Wildgoose, G. G.; Compton, R. G. Electrocatalysis at Graphite and Carbon Nanotube Modified Electrodes: Edge-Plane Sites and Tube Ends Are the Reactive Sites. *Chem. Commun. (Cambridge, U. K.)* **2005**, 829−841.
(10) Edwards, M. A.; Bertoncello, P.; Unwin, P. R. Slow Diffusion Reveals the Intrinsic Electrochemical Activity of Basal Plane Highly Oriented Pyrolytic Graphite Electrodes. *J. Phys. Chem. C* **2009**, *113*, 9218−9223.
(11) Patel, A. N.; Collignon, M. G.; O'Connell, M. A.; Hung, W. O. Y.; McKelvey, K.; MacPherson, J. V.; Unwin, P. R. A New Ciew of Electrochemistry at Highly Oriented Pyrolytic Graphite. *J. Am. Chem. Soc.* **2012**, *134*, 20117−20130.
(12) Tan, C.; Rodríguez-López, J.; Parks, J. J.; Ritzert, N. L.; Ralph, D. C.; Abruña, H. D. Reactivity of Monolayer Chemical Vapor Deposited Graphene Imperfections Studied Using Scanning Electrochemical Microscopy. *ACS Nano* **2012**, *6*, 3070−3079.
(13) Davies, T. J.; Hyde, M. E.; Compton, R. G. Nanotrench Arrays Reveal Insight Into Graphite Electrochemistry. *Angew. Chem., Int. Ed.* **2005**, *44*, 5121−5126.
(14) Zhong, J.-H.; Zhang, J.; Jin, X.; Liu, J.-Y.; Li, Q.; Li, M.-H.; Cai, W.; Wu, D.-Y.; Zhan, D.; Ren, B. Quantitative Correlation Between Defect Density and Heterogeneous Electron Transfer Rate of Single Layer Graphene. *J. Am. Chem. Soc.* **2014**, *136*, 16609−16617.
(15) Li, W.; Tan, C.; Lowe, M. A.; Abruña, H. D.; Ralph, D. C. Electrochemistry of Individual Monolayer Graphene Sheets. *ACS Nano* **2011**, *5*, 2264−2270.
(16) Wain, A. J.; Pollard, A. J.; Richter, C. High-Resolution Electrochemical and Topographical Imaging Using Batch-Fabricated Cantilever Probes. *Anal. Chem.* **2014**, *86*, 5143−5149.
(17) Zhang, G.; Kirkman, P. M.; Patel, A. N.; Cuharuc, A. S.; McKelvey, K.; Unwin, P. R. Molecular Functionalization of Graphite Surfaces: Basal Plane Versus Step Edge Electrochemical Activity. *J. Am. Chem. Soc.* **2014**, *136*, 11444−11451.
(18) Valota, A. T.; Toth, P. S.; Kim, Y.-J.; Hong, B. H.; Kinloch, I. A.; Novoselov, K. S.; Hill, E. W.; Dryfe, R. A. W. Electrochemical Investigation of Chemical Vapour Deposition Monolayer and Bilayer Graphene on the Microscale. *Electrochim. Acta* **2013**, *110*, 9−15.
(19) Toth, P. S.; Valota, A.; Velický, M.; Kinloch, I.; Novoselov, K.; Hill, E. W.; Dryfe, R. A. W. Electrochemistry in a Drop: A Study of the Electrochemical Behaviour of Mechanically Exfoliated Graphene on Photoresist Coated Silicon Substrate. *Chem. Sci.* **2014**, *5*, 582−589.
(20) Lai, S. C. S.; Patel, A. N.; McKelvey, K.; Unwin, P. R. Definitive Evidence for Fast Electron Transfer at Pristine Basal Plane Graphite from High-Resolution Electrochemical Imaging. *Angew. Chem., Int. Ed.* **2012**, *51*, 5405−5408.
(21) Klintenberg, M.; Lebègue, S.; Ortiz, C.; Sanyal, B.; Fransson, J.; Eriksson, O. Evolving Properties of Two-Dimensional Materials: From Graphene to Graphite. *J. Phys.: Condens. Matter* **2009**, *21*, 335502.
(22) Ooi, N.; Rairkar, A.; Adams, J. B. Density Functional Study of Graphite Bulk and Surface Properties. *Carbon* **2006**, *44*, 231−242.
(23) McCreery, R. L.; McDermott, M. T. Comment on Electrochemical Kinetics at Ordered Graphite Electrodes. *Anal. Chem.* **2012**, *84*, 2602−2605.
(24) McDermott, M. T.; McCreery, R. L. Scanning Tunneling Microscopy of Ordered Graphite and Glassy Carbon Surfaces: Electronic Control of Quinone Adsorption. *Langmuir* **1994**, *10*, 4307−4314.
(25) Niimi, Y.; Matsui, T.; Kambara, H.; Tagami, K.; Tsukada, M.; Fukuyama, H. Scanning Tunneling Microscopy and Spectroscopy of the Electronic Local Density of States of Graphite Surfaces near Monoatomic Step Edges. *Phys. Rev. B: Condens. Matter Mater. Phys.* **2006**, *73*, 085421.
(26) Zhang, X.; Yazyev, O. V.; Feng, J.; Xie, L.; Tao, C.; Chen, Y.-C.; Jiao, L.; Pedramrazi, Z.; Zettl, A.; Louie, S. G.; et al. Experimentally Engineering the Edge Termination of Graphene Nanoribbons. *ACS Nano* **2013**, *7*, 198−202.
(27) Brownson, D. A. C.; Munro, L. J.; Kampouris, D. K.; Banks, C. E. Electrochemistry of Graphene: Not such a Beneficial Electrode Material? *RSC Adv.* **2011**, *1*, 978−988.
(28) Kobayashi, K. Electronic Structure of a Stepped Graphite Surface. *Phys. Rev. B: Condens. Matter Mater. Phys.* **1993**, *48*, 1757−1760.
(29) Rice, R. J.; Pontikos, N. M.; McCreery, R. I. Quantitative Correlations of Heterogeneous Electron-Transfer Kinetics with Surface Properties of Glassy Carbon Electrodes. *J. Am. Chem. Soc.* **1990**, *112*, 4617−4622.
(30) Unwin, P. R. Concluding Remarks: There's Nowt so Queer As Carbon Electrodes. *Faraday Discuss.* **2014**, *172*, 521−532.
(31) McCreery, R. L.; Cline, K. K.; McDermott, C. A.; McDermott, M. T. Control of Reactivity at Carbon Electrode Surfaces. *Colloids Surf., A* **1994**, *93*, 211−219.
(32) Davies, T. J.; Moore, R. R.; Banks, C. E.; Compton, R. G. The Cyclic Voltammetric Response of Electrochemically Heterogeneous Surfaces. *J. Electroanal. Chem.* **2004**, *574*, 123−152.
(33) Williams, C. G.; Edwards, M. A.; Colley, A. L.; Macpherson, J. V.; Unwin, P. R. Scanning Micropipet Contact Method for High-Resolution Imaging of Electrode Surface Redox Activity. *Anal. Chem.* **2009**, *81*, 2486−2495.

DOI: 10.1021/acs.jpcc.9b01010
J. Phys. Chem. C 2019, 123, 11677−11685

(34) Patten, H. V.; Velický, M.; Clark, N.; Muryn, C. A.; Kinloch, I. A.; Dryfe, R. A. W. Electrochemistry of Well-Defined Graphene Samples: Role of Contaminants. *Faraday Discuss.* **2014**, *172*, 261−271.
(35) Velický, M.; Bissett, M. A.; Toth, P. S.; Patten, H. V.; Worrall, S. D.; Rodgers, A. N. J.; Hill, E. W.; Kinloch, I. A.; Novoselov, K. S.; Georgiou, T.; et al. Electron Transfer Kinetics on Natural Crystals of MoS_2 and Graphite. *Phys. Chem. Chem. Phys.* **2015**, *17*, 17844−17853.
(36) McCreery, R. L. Advanced Carbon Electrode Materials for Molecular Electrochemistry. *Chem. Rev. (Washington, DC, U. S.)* **2008**, *108*, 2646−2687.
(37) Bard, A. J.; Faulkner, L. R. *Electrochemical Methods. Fundamentals and Applications*, 2nd ed.; John Wiley & Sons, Inc.: New York, 2001.
(38) Zhang, G.; Cuharuc, A. S.; Güell, A. G.; Unwin, P. R. Electrochemistry at Highly Oriented Pyrolytic Graphite (HOPG): Lower Limit for the Kinetics of Outer-Sphere Redox Processes and General Implications for Electron Transfer Models. *Phys. Chem. Chem. Phys.* **2015**, *17*, 11827−11838.
(39) Li, Z.; Kozbial, A.; Nioradze, N.; Parobek, D.; Shenoy, G. J.; Salim, M.; Amemiya, S.; Li, L.; Liu, H. Water Protects Graphitic Surface from Airborne Hydrocarbon Contamination. *ACS Nano* **2016**, *10*, 349−359.
(40) Velický, M.; Bradley, D. F.; Cooper, A. J.; Hill, E. W.; Kinloch, I. A.; Mishchenko, A.; Novoselov, K. S.; Patten, H. V.; Toth, P. S.; Valota, A. T.; et al. Electron Transfer Kinetics on Mono- and Multilayer Graphene. *ACS Nano* **2014**, *8*, 10089−10100.
(41) Robinson, R. S.; Sternitzke, K.; McDermott, M. T.; McCreery, R. L. Morphology and Electrochemical Effects of Defects on Highly Oriented Pyrolytic Graphite. *J. Electrochem. Soc.* **1991**, *138*, 2412−2418.
(42) Nioradze, N.; Chen, R.; Kurapati, N.; Khvataeva-Domanov, A.; Mabic, S.; Amemiya, S. Organic Contamination of Highly Oriented Pyrolytic Graphite As Studied by Scanning Electrochemical Microscopy. *Anal. Chem.* **2015**, *87*, 4836−4843.
(43) Velický, M.; Toth, P. S.; Rakowski, A. M.; Rooney, A. P.; Kozikov, A.; Woods, C. R.; Mishchenko, A.; Fumagalli, L.; Yin, J.; Zólyomi, V.; et al. Exfoliation of Natural van der Waals Heterostructures to a Single Unit Cell Thickness. *Nat. Commun.* **2017**, *8*, 14410.
(44) Klingler, R. J.; Kochi, J. K. Electron-Transfer Kinetics from Cyclic Voltammetry. Quantitative Description of Electrochemical Reversibility. *J. Phys. Chem.* **1981**, *85*, 1731−1741.
(45) Lavagnini, I.; Antiochia, R.; Magno, F. An Extended Method for the Practical Evaluation of the Standard Rate Constant from Cyclic Voltammetric Data. *Electroanalysis* **2004**, *16*, 505−506.
(46) Ray, K.; McCreery, R. L. Spatially Resolved Raman Spectroscopy of Carbon Electrode Surfaces: Observations of Structural and Chemical Heterogeneity. *Anal. Chem.* **1997**, *69*, 4680−4687.
(47) Xiao, J.; Zhang, L.; Zhou, K.; Li, J.; Xie, X.; Li, Z. Anisotropic Friction Behaviour of Highly Oriented Pyrolytic Graphite. *Carbon* **2013**, *65*, 53−62.
(48) Zou, Y.; Walton, A. S.; Kinloch, I. A.; Dryfe, R. A. W. Investigation of the Differential Capacitance of Highly Ordered Pyrolytic Graphite as a Model Material of Graphene. *Langmuir* **2016**, *32*, 11448−11455.
(49) Gerischer, H. An Interpretation of the Double Layer Capacity of Graphite Electrodes in Relation to the Density of States at the Fermi Level. *J. Phys. Chem.* **1985**, *89*, 4249−4251.
(50) Velický, M.; Donnelly, G. E.; Hendren, W. R.; McFarland, S.; Scullion, D.; DeBenedetti, W. J. I.; Correa, G. C.; Han, Y.; Wain, A. J.; Hines, M. A.; et al. Mechanism of Gold-Assisted Exfoliation of Centimeter-Sized Transition-Metal Dichalcogenide Monolayers. *ACS Nano* **2018**, *12*, 10463−10472.
(51) Trasatti, S. The Absolute Electrode Potential: An Explanatory Note (Recommendations 1986). *J. Electroanal. Chem. Interfacial Electrochem.* **1986**, *209*, 417−428.
(52) Ergun, S.; Yasinsky, J. B.; Townsend, J. R. Transverse and Longitudinal Optical Properties of Graphite. *Carbon* **1967**, *5*, 403−408.
(53) Klein, C. A.; Straub, W. D. Carrier Densities and Mobilities in Pyrolytic Graphite. *Phys. Rev.* **1961**, *123*, 1581−1583.
(54) Yuan, W.; Zhou, Y.; Li, Y.; Li, C.; Peng, H.; Zhang, J.; Liu, Z.; Dai, L.; Shi, G. The Edge- and Basal-Plane-Specific Electrochemistry of a Single-Layer Graphene Sheet. *Sci. Rep.* **2013**, *3*, 2248.
(55) Iamprasertkun, P.; Hirunpinyopas, W.; Keerthi, A.; Wang, B.; Radha, B.; Bissett, M. A.; Dryfe, R. A. W. Capacitance of Basal Plane and Edge-Oriented Highly Ordered Pyrolytic Graphite: Specific Ion Effects. *J. Phys. Chem. Lett.* **2019**, *10*, 617−623.
(56) Grahame, D. C. The Electrical Double Layer and the Theory of Electrocapillarity. *Chem. Rev. (Washington, DC, U. S.)* **1947**, *41*, 441−501.
(57) Rosen, M.; Flinn, D. R.; Schuldiner, S. Double Layer Capacitance on Platinum in 1 M H_2SO_4 from the Reversible Hydrogen Potential to the Oxygen Formation Region. *J. Electrochem. Soc.* **1969**, *116*, 1112−1116.
(58) Matsumoto, M.; Manako, T.; Imai, H. Electrochemical STM Investigation of Oxidative Corrosion of the Surface of Highly Oriented Pyrolytic Graphite. *J. Electrochem. Soc.* **2009**, *156*, B1208−B1211.
(59) Chen, P.; Fryling, M. A.; McCreery, R. L. Electron Transfer Kinetics at Modified Carbon Electrode Surfaces: The Role of Specific Surface Sites. *Anal. Chem.* **1995**, *67*, 3115−3122.
(60) Feldberg, S. W.; Sutin, N. Distance Dependence of Heterogeneous Electron Transfer Through the Nonadiabatic and Adiabatic Regimes. *Chem. Phys.* **2006**, *324*, 216−225.
(61) Amatore, C.; Savéant, J. M.; Tessier, D. Charge Transfer at Partially Blocked Surfaces. A Model for the Case of Microscopic Active and Inactive Sites. *J. Electroanal. Chem. Interfacial Electrochem.* **1983**, *147*, 39−51.
(62) Dresselhaus, M. S.; Dresselhaus, G.; Fischer, J. E. Graphite Intercalation Compounds: Electronic Properties in the Dilute Limit. *Phys. Rev. B* **1977**, *15*, 3180−3192.
(63) Slonczewski, J. C.; Weiss, P. R. Band Structure of Graphite. *Phys. Rev.* **1958**, *109*, 272−279.
(64) Kneten, K. R.; McCreery, R. L. Effects of Redox System Structure on Electron-Transfer Kinetics at Ordered Graphite and Glassy Carbon Electrodes. *Anal. Chem.* **1992**, *64*, 2518−2524.
(65) Miller, C.; Graetzel, M. Electrochemistry at ω-Hydroxy thiol Coated Electrodes. 2. Measurement of the Density of Electronic States Distributions for Several Outer-Sphere Redox Couples. *J. Phys. Chem.* **1991**, *95*, 5225−5233.
(66) Slowinski, K.; Slowinska, K. U.; Majda, M. Electron Tunneling Across Hexadecanethiolate Monolayers on Mercury Electrodes: Reorganization Energy, Structure, and Permeability of the Alkane/Water Interface. *J. Phys. Chem. B* **1999**, *103*, 8544−8551.
(67) Royea, W. J.; Hamann, T. W.; Brunschwig, B. S.; Lewis, N. S. A Comparison Between Interfacial Electron-Transfer Rate Constants at Metallic and Graphite Electrodes. *J. Phys. Chem. B* **2006**, *110*, 19433−19442.
(68) Kobayashi, Y.; Fukui, K.-i.; Enoki, T.; Kusakabe, K.; Kaburagi, Y. Observation of Zigzag and Armchair Edges of Graphite Using Scanning Tunneling Microscopy and Spectroscopy. *Phys. Rev. B: Condens. Matter Mater. Phys.* **2005**, *71*, 193406.
(69) Spain, I. L.; Ubbelohde, A. R.; Young, D. A. Electronic Properties of Well Oriented Graphite. *Philos. Trans. R. Soc., A* **1967**, *262*, 345−386.

DOI: 10.1021/acs.jpcc.9b01010
J. Phys. Chem. C 2019, 123, 11677−11685